NPL REPORT ENG 41

Application of the optical transfer function in X-ray computed tomography – a review

N FLAY, R K LEACH

NOVEMBER 2012

Application of the optical transfer function in X-ray computed tomography

Nadia Flay, Richard Leach
Engineering Measurement Division

ABSTRACT

In this report the application of the optical transfer function for X-ray computed tomography is reviewed. Brief introductions to the optical transfer function, X-ray computed tomography and the concept of spatial resolution are presented. The use of the modulation transfer function as a measure of the spatial resolution in X-ray computed tomography is discussed. Three methods for calculating the modulation transfer function are briefly reviewed. In conclusion, some of the gaps in the application of the optical transfer function in X-ray computed tomography are identified and future areas of research are proposed.

ISSN 1754-2987

National Physical Laboratory
Hampton Road, Teddington, Middlesex, TW11 0LW

This work was funded by the BIS National Measurement System Engineering and Flow Metrology Programme 2011 – 2014. We also thank Dr Matthew Foreman (Imperial College, UK), Claudiu Giusca and James Claverley (National Physical Laboratory, UK), and Prof Ian Sinclair and Dr Kevin Cross (University of Southampton, UK) for their contributions.

Approved on behalf of NPLML by Dr Andrew Lewis, Science Area Leader, Dimensional Metrology.

CONTENTS

FIGURES

1 INTRODUCTION TO THE OPTICAL TRANSFER FUNCTION

To be able to describe the performance of an imaging system fully, many different parameters must be taken into consideration. Some of these parameters are relevant to a variety of systems and others are specific to a particular system. One of the most important characteristics of an imaging system is its ability to reproduce faithfully the relative intensity distribution of the original object in the final image. The parameter that is now widely used to describe this aspect of imaging is the optical transfer function (OTF) [1].

The OTF is defined as a measure of how the contrast and phase of a sinewave grating pattern (*i.e.* one where the transmittance perpendicular to the direction of the grating lines varies sinusoidally) is reproduced by the imaging system [1]. The contrast component of the OTF is called the modulation transfer function (MTF) and the phase component is called the phase transfer function (PTF). This relationship can be expressed with the following

$$\mathrm{OTF}\,(\omega) = T\,(\omega)\,\exp[i\,\phi\,(\omega)] \tag{1}$$

where T is the MTF, φ is the PTF and ω is a spatial frequency [2]. In other words [1]

$$\mathrm{OTF}\,(\omega) = \mathrm{MTF}(\omega)\,\exp[i\,\mathrm{PTF}(\omega)], \tag{2}$$

and it follows that

$$\mathrm{MTF}(\omega) = |\mathrm{OTF}\,(\omega)|. \tag{3}$$

The relationship between the OTF, the MTF and the PTF at a given spatial frequency is represented graphically in figure 1.

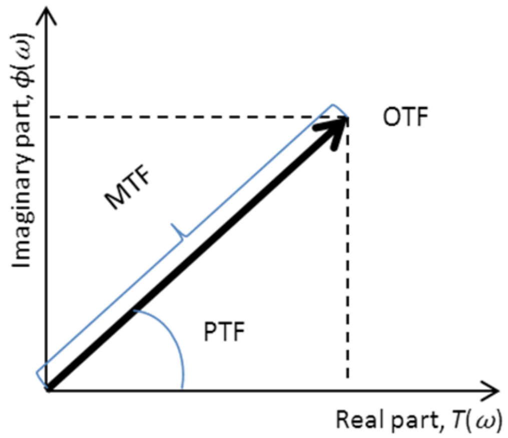

Figure 1. Depiction of the OTF in the complex plane, showing its relationship with the MTF and the PTF (adapted from [3])

For the OTF to be valid, the imaging system must be linear and space invariant. Linearity is a property distinguished by two basic characteristics: the output corresponding to a sum of inputs is equal to the sum of outputs corresponding to the inputs acting separately; and multiplication of the input by a constant multiplies the output by the same constant. Space invariance requires that the image of a point retains its shape or size as the object point is moved in the object plane [4].

In most cases only the MTF part of the OTF is used to describe the performance of an imaging system. The main reason for omitting the PTF is that significant changes in the PTF predominantly occur at higher spatial frequencies where the MTF has fallen to relatively low levels (see figure 2), and the effect of the changing phase has limited impact on the image quality [1]. In X-ray computed tomography (XCT) systems the phase information is not preserved [5], but can be retrieved using a number of techniques [6].

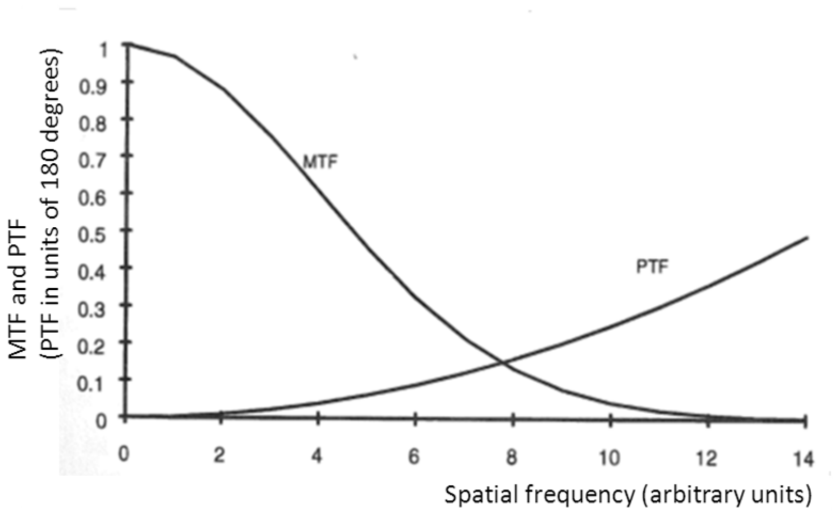

Figure 2. Plot of the MTF and the PTF against spatial frequency for a typical optical system [1]

In analysing the performance of an imaging system, it is important to take into account the degree of coherence of the source. Coherence of electromagnetic waves is a property that enables their interference. It has two aspects: temporal and spatial. Temporal coherence is the measure of correlation in phase values of electromagnetic waves at different times at a given point in space. Temporal coherence describes how monochromatic the source is. Spatial coherence is the measure of correlation in phase values at different points in space at a given time [7].

The OTF is the transfer function of a spatially incoherent imaging system and is the Fourier transform of the intensity point-spread function (PSF). In a spatially coherent system, the transfer function is referred to as the amplitude transfer function (ATF) and is the Fourier transform of the amplitude PSF [8], [9]. In industrial XCT imaging systems, the X-ray source is polychromatic in nature (see section 2) and is, therefore, assumed to be spatially and temporally incoherent.

2 INTRODUCTION TO XCT

XCT is a non-destructive imaging technique that uses the propagating properties of X-rays to examine the external and internal geometries of an object. Over the last three decades XCT has revolutionised diagnostic medicine and found a wide range of applications within many industries. In recent years, thanks to increasing technical sophistication, XCT has successfully entered the field of industrial dimensional metrology [10].

In XCT imaging systems, as the X-rays leave the source and pass through an object, a series of detectors measure the extent to which the X-rays are attenuated by the object. The process of attenuation is governed by the Lambert-Beers law. For a simplified case of a monochromatic source, where X-rays pass through a homogeneous material, the law can be expressed mathematically [5]

$$I = I_0 \exp(-\mu \cdot \Delta x) \tag{4}$$

where I and I_0 represent the transmitted and incident X-ray intensities respectively, μ is the linear attenuation coefficient of the material, and Δx is the thickness of the material (see figure 3a). By determining the ratio I_0/I for a large number of ray paths through the object and taking their logarithms, an attenuation profile, often referred to as a projection, P, is then obtained

$$P = \ln \frac{I_0}{I} = \mu \cdot \Delta x. \tag{5}$$

If the object is inhomogeneous, the overall attenuation characteristics can be obtained by dividing the object into thin slices, where each slice is considered to be uniform (as shown in figure 3b). Mathematically this process is expressed as follows

$$I = I_0 \exp(-\mu_1 \Delta x) \exp(-\mu_2 \Delta x) \ldots \exp(-\mu_\mathrm{n} \Delta x) = I_0 \exp\left(-\sum_{n=1}^{N} \mu_n \Delta x\right), \tag{6}$$

then

$$P = \ln \frac{I_0}{I} = \sum_{n=1}^{N} \mu_n \Delta x \tag{7}$$

and, as Δx approaches zero, the above summation becomes as integration over the length of the object

$$P = \ln \frac{I_0}{I} = \int_L \mu(x) dx \,. \tag{8}$$

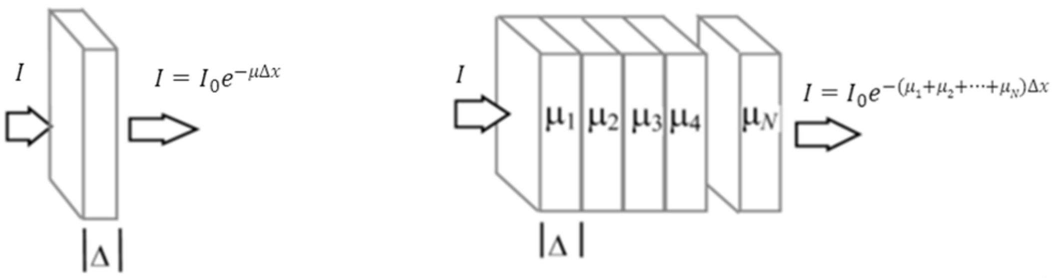

(a) **(b)**

Figure 3. Illustration of material attenuation for a monochromatic X-ray beam. (a) Attenuation by a homogeneous object. (b) Attenuation by an inhomogeneous object [5]

In most modern day XCT systems the X-ray source is not monochromatic but polychromatic in nature (see figure 4). X-ray photons are produced when a target material is bombarded by high-speed electrons. X-rays are generated in three main ways. The first occurs when a high-speed electron approaches an atomic nucleus and is decelerated, giving rise to Bremsstrahlung radiation (German term for “breaking radiation”). This type of radiation is responsible for white radiation, which covers the entire range of the energy spectrum and is the dominant X-ray production process (figure 4a) [11].

The second type of interaction occurs when an incoming electron collides directly with one of the shell electrons, creating an electron vacancy. As this vacancy is filled with an electron from an outer shell, X-rays of discrete or characteristic energies are produced (figure 4b). This characteristic radiation is a property of the target material [12]. The third type of interaction occurs when an electron collides directly with a nucleus and its entire energy appears as Bremsstrahlung. The X-ray energy produced by this interaction represents the upper energy limit in the X-ray spectrum [5].

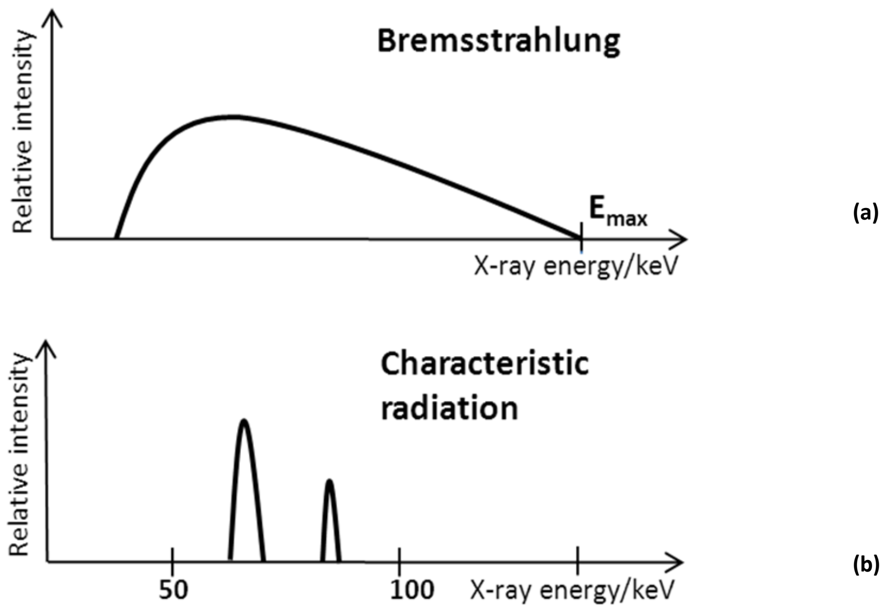

Figure 4. Typical X-ray spectra: (a) Bremsstrahlung radiation, (b) characteristic radiation [11]

Since the produced X-ray beam covers a broad spectrum, the linear attenuation coefficients are no longer associated with a single energy, but rather with an effective energy that is constantly changing along the ray path [13]. The reason for this change is that the low-energy X-ray photons are preferentially attenuated, as a result the X-ray beam spectrum becomes harder (averages a higher energy) as it passes through an object. This is reflected in the Lambert-Beers law for a polychromatic source [5]

$$I = I_0 \int \Omega(E) \exp(-\int \mu_E(x)dx)dE \tag{9}$$

where $\Omega(E)$ represents the incident X-ray spectrum, the area under $\Omega(E)$ equals unity, and $\mu_E(x)$ is the linear attenuation coefficient of the object at the same energy. The projection then becomes

$$P = \log\frac{I_0}{I} = -\log(\int \Omega(E) \exp\left(-\int \mu_E(x)dx\right) dE) . \tag{10}$$

A simple setup for a pencil beam XCT system is shown in figure 5.

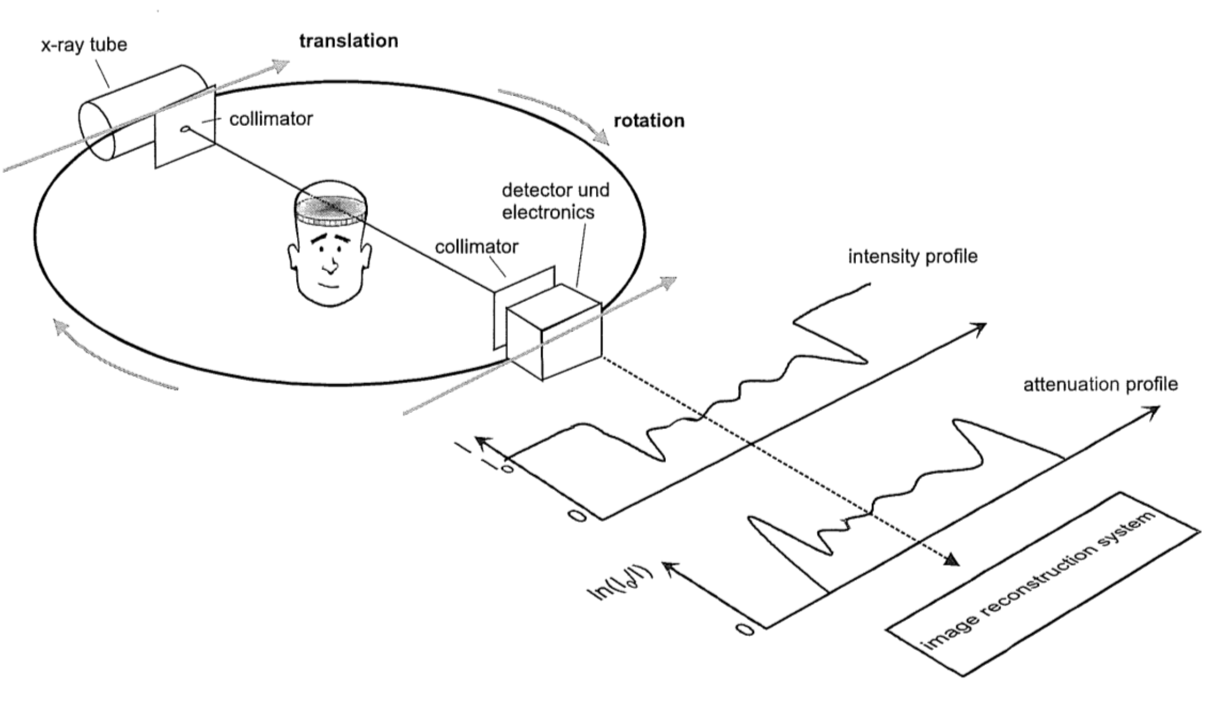

Figure 5. The simplest case of XCT system, where the object's attenuation is measured with a pencil beam from many different orientations [14]

Multiple sets of projections from an object are acquired from a range of angular orientations, and the subsequent mathematical reconstruction of these data leads to a 3D model of an object. Most modern XCT scanners typically measure 800 to 1500 projections with 600 to 1200 data points per projection [14]. In-depth discussions of XCT processes are presented, for example, in [5], [12], [13], [14], [15], [16], [17].

3 SPATIAL RESOLUTION

There are three main parameters that affect the image quality in XCT: spatial resolution, statistical noise and artefacts [13], [15]. Spatial resolution, often referred to as high-contrast resolution, describes the ability of an imaging system to resolve two closely placed objects [5].

3.1 CLASSICAL CRITERIA OF THE SPATIAL RESOLUTION

In the past, several criteria for the two-point resolution for imaging systems have been suggested [8], [18], [19], [20]. Arguably, the most famous criterion was proposed by Lord Rayleigh and is known as the classical Rayleigh criterion. It states that two point sources are just resolved if the diffraction maximum of one source coincides with the diffraction minimum of the other (see figure 6) [21].

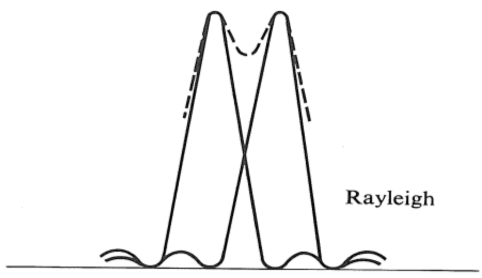

Figure 6. The Rayleigh criterion for spatial resolution [22]

If Δl is the centre-to-centre separation of the images, the limit of resolution of an imaging system is given by

$$\Delta l_{\min} = 1.22 f\lambda/D \tag{11}$$

where f is the focal length of the optical system, λ is the wavelength of the light and D is the diameter of the imaging lens's aperture [22]. Although the Rayleigh criterion is useful, it is somewhat arbitrary, and is based on the resolving capabilities of the human eye [8]. In Rayleigh's own words it is a convenient rule on account of its simplicity and is sufficiently accurate in view of the necessary uncertainty as to what exactly is meant by resolution [23].

An alternative resolution was proposed by Sparrow. As the distance between the two point sources in figure 6 is decreased even further, the central minimum that exists between two peaks at the Rayleigh criterion disappears. The resultant maximum has a broad flat top as in figure 7. The angular separation corresponding to this configuration is the Sparrow limit. In other words, at the centre, the second derivative of the total distribution of the irradiance function is zero - there is no change in slope [22].

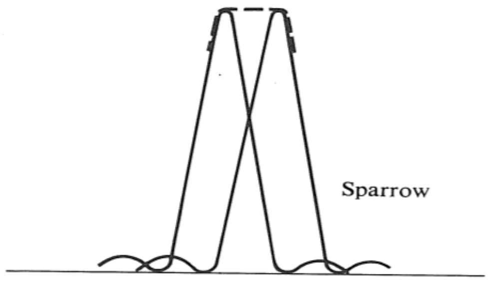

Figure 7. The Sparrow criterion for spatial resolution [22]

Both Rayleigh and Sparrow criteria assume incoherent sources of radiation in their original context. Later these concepts were extended to coherent and partially coherent sources [21], [24], [25], [26]. Such classical criteria provide resolution limits for calculated images that do not take noise or other errors into account [8]. Since such images do not exist in reality, it has been suggested that it is of more value to consider the resolution of the detected images rather than those of the calculated ones [27].

3.2 SPATIAL RESOLUTION IN XCT

3.2.1 Direct measurement of the spatial resolution

With technological advances in imaging systems, the concept of spatial resolution and its limits has been widely used as a quality criterion. Spatial resolution is generally quantified in terms of the smallest separation at which two points can be distinguished as separate entities [15], in many imaging systems, including XCT, a direct measurement of the spatial resolution is performed using hole or line-pair test patterns (figures 8 and 9).

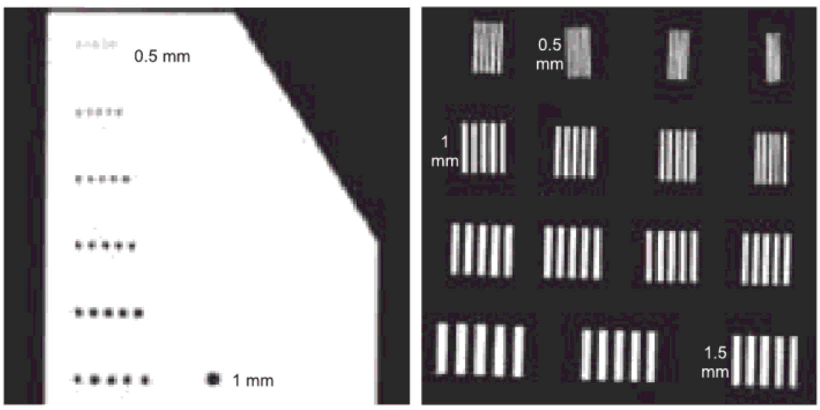

Figure 8. Drilled hole pattern bar (left) and bar pattern (right) [14]

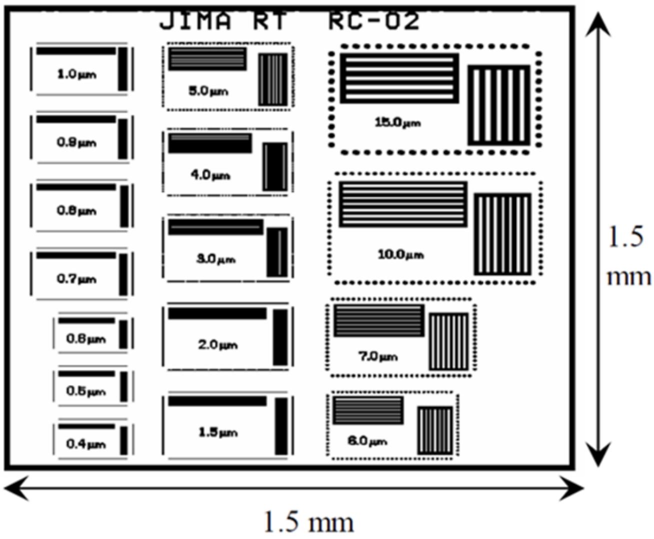

Figure 9. Jima line and space test pattern for XCT [28]

These test objects consist of a series of multiple hole or bar patterns that gradually reduce in size, *i.e.* increase in spatial frequency (the spatial frequency is the reciprocal of the periodicity of the grating). A dark and bright hole or bar pair constitutes one cycle on the object and is commonly measured in line-pairs per millimetre. Since even an ideal imaging system is limited by diffraction effects, the image of the test patterns will be blurred (see section 4.1 for more detail). As the width of the bars and their separation become less, a limit is reached where the fine-line structure will no longer be discernible to the human eye. This point is the resolution limit of the imaging system, or the spatial frequency cut-off [22].

Although the method of scanning the line-pair test patterns is easy to perform and to interpret, there are a number of drawbacks associated with it. The most significant drawback is that it relies on a subjective evaluation of the spatial resolution by the user and his or her visual ability, and hence can produce different results for different users [1], [14], [29]. Another issue is the mechanical difficulties in manufacturing and calibration of such line-pair patterns, as well as their high cost. It is important to mention that this method of using the line-pair test patterns evaluates only the in-plane spatial resolution (see section 3.2.2).

3.2.2 The MTF as the measure of the spatial resolution

The measure of the spatial resolution that is considered to be objective involves calculations of the MTF, the contrast component of the OTF [13], [14].

If a sinusoidal intensity distribution in the object plane is imaged by a linear nonisotropic imaging system, the intensity distribution in the image plane will also be sinusoidal with the same spatial frequency as the object. However, because of the system's imperfections and diffraction effects, the amplitude in the image distribution will be reduced and shifted laterally. The reduction in the amplitude indicates the loss in the contrast of the system (figure 10) [4].

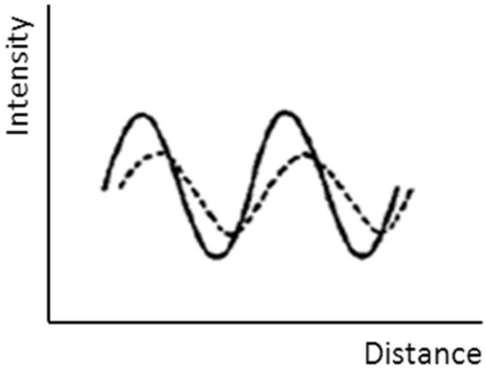

Figure 10. Sinusoidal intensity distribution in space. Solid line is input distribution of a given frequency. Dotted line is output distribution from a linear nonisotropic imaging system [4]

Contrast or modulation is defined by

$$\text{Modulation} = \frac{I_{max} - I_{min}}{I_{max} + I_{min}} \tag{12}$$

where I_{max} and I_{min} are the maximum and minimum intensities respectively (see figure 11). Contrast is effectively a measure of how readily the fluctuations of the sinusoidal wave are discernible against the dc background [22].

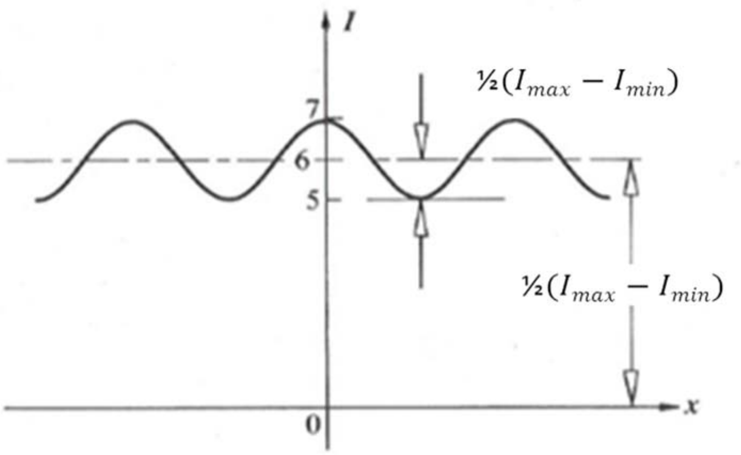

Figure 11. Illustration of the sinusoidal intensity distribution in space (adapted from [22])

The MTF is defined as the ratio of the image modulation, M_{img}, to the object modulation, M_{obj}, at all spatial frequencies [30]

$$\text{MTF} = \frac{M_{img}}{M_{obj}}. \tag{13}$$

The relationship between the phase of the object, φ_{obj}, and the phase of the image, φ_{img}, can be represented as follows [1]

$$\varphi_{img}(\omega) = \varphi_{obj}(\omega) + \mathrm{PTF}(\omega) \tag{14}$$

where ω is the spatial frequency. In conventional XCT systems the phase information is not preserved [5].

It is important to distinguish between the *x*/*y*-scan plane (in-plane) spatial resolution, represented by the MTF, and the spatial resolution in the *z*-direction, represented by the slice sensitivity profile (SSP) (see section 5), since they depend on different factors. The spatial resolution in the scan plane is influenced by the focal spot size and shape, scanner geometry, detector aperture and reconstruction algorithm. These factors are discussed in detail in [5] and [14]. The combination of the scan plane and the z-direction spatial resolutions give a three-dimensional (3D) evaluation of the spatial resolution.

In XCT, another type of resolution, the low-contrast resolution needs to be taken into account. The low-contrast resolution describes the ability of an imaging system to distinguish a low-contrast object from its background [5]. Its detectability is determined primarily by the noise level in the image and the signal-to-noise ratio (SNR) of the system [14]. The low-contrast resolution will not be further discussed in this report, since it does not involve the calculation of the MTF.

The MTF can be calculated in a variety of ways. At present, there is no internationally accepted standard for evaluating spatial resolution [12], hence manufacturers use different procedures and techniques for calculating the MTF to obtain the values for the spatial resolution that would give them the best results.

4 PROCEDURES FOR OBTAINING THE MTF IN THE *X*/*Y* SCAN PLANE

4.1 INTRODUCTION TO THE PSF AND ITS RELATIONSHIP TO THE MTF

In an ideal imaging system an infinitely small point in the object plane would be represented by an identical point in the image plane. However, in real XCT imaging systems, the system's imperfections and diffraction effects cause the image to be blurred. This blurring is described by a PSF [13], [22]. The PSF is defined as the response of the system to an ideal point object or Dirac delta function, $\delta(x, y)$, thus

$$\delta(x, y) = 0, \quad \text{for } (x, y) \neq (0,0), \tag{15}$$

$$\iint_{-\infty}^{+\infty} \delta(x, y)dxdy = 1, \qquad \text{and} \tag{16}$$

$$\iint_{-\infty}^{+\infty} f(x, y)\delta(x - x_0, y - y_0)dxdy = f(x_0, y_0) \tag{17}$$

where $f(x, y)$ is continuous at (x_0, y_0). $\delta(x, y)$ has an infinitely small width and an infinitely large magnitude. The area under the function equals unity [5].

Figure 12 is a schematic representation of a response of an imaging system to two point objects [4].

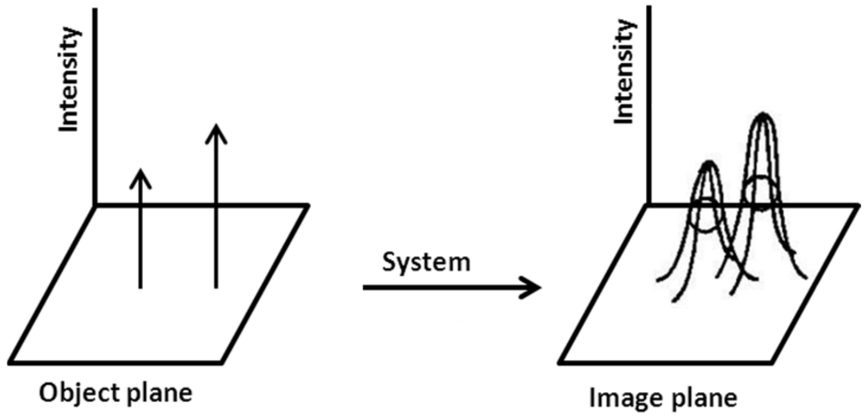

Figure 12. A schematic representation of a response of an imaging system to two point objects [4]

Any two-dimensional continuous object can be thought to consist of an infinite number of point sources of different intensities. Hence, if the input intensity distribution and the PSF of the imaging system are known, the output intensity in the image could be determined. Therefore, the PSF is the general transfer characteristic of a linear, space invariant imaging system. If the PSF possesses rotational symmetry as in figure 12, the imaging system is isotropic [4].

Mathematically, the image function, $I(x, y)$, results from the convolution of the object function $O(x, y)$ with the PSF(x, y) [31]

$$I(x, y) = O(x, y) \otimes \mathrm{PSF}(x, y). \quad (18)$$

The process of convolution is discussed in more detail in [4], [5], [32]. Just as the PSF is the transfer characteristic of the linear, space invariant imaging system in the real space domain, the MTF and the PTF are the transfer characteristics in the spatial frequency domain. In isotropic systems the phase shift is zero, and the MTF completely describes the transfer characteristics of the system [4]. In such imaging systems the MTF is the Fourier transform of a profile through a PSF [13], [33]. The relationship between the spatial and the frequency domains is represented graphically in figure 13.

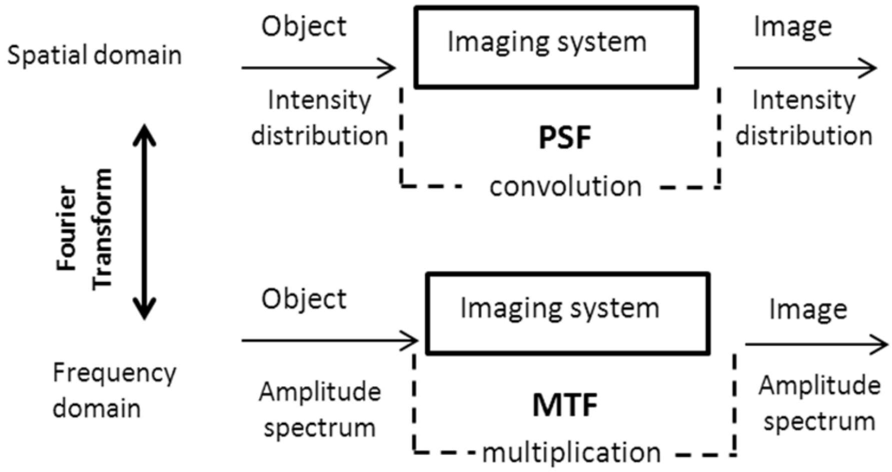

Figure 13. Representation of the relationship between the spatial domain and the spatial frequency domain for incoherent imaging systems (adapted from [4])

More rigorous discussions about the spatial domain, the spatial frequency domain and Fourier transform theory are presented in [2], [3], [5], [22].

4.2 CALCULATING THE MTF FROM THE PSF

As previously mentioned, the MTF of an imaging system can be obtained by calculating the magnitude of the Fourier transform of its PSF. Since the ideal point object does not exist, a high-density wire with a diameter much smaller than the limiting spatial resolution is often used to approximate the PSF in XCT. One such example is described elsewhere [5]. The GE Performance™ phantom in figure 7, which uses a 0.08 mm diameter tungsten wire submerged in water, is imaged with an XCT instrument.

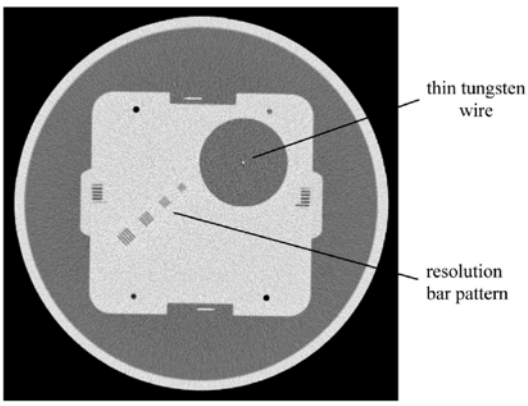

Figure 14. Reconstructed image of a GE Performance™ phantom [5]

A targeted reconstruction of the image around the wire is then performed using the standard algorithm to approximate the PSF. For accurate PSF measurement, the background variations in the wire image due to beam-hardening, focal drift and other factors are removed by fitting a smooth function to the water region around the wire. Next, a 2D Fourier transform of the wire image is performed, and the magnitude of the 2D function, the estimation of the system's MTF, is obtained (see figure 15). In this process, the phase information is not preserved.

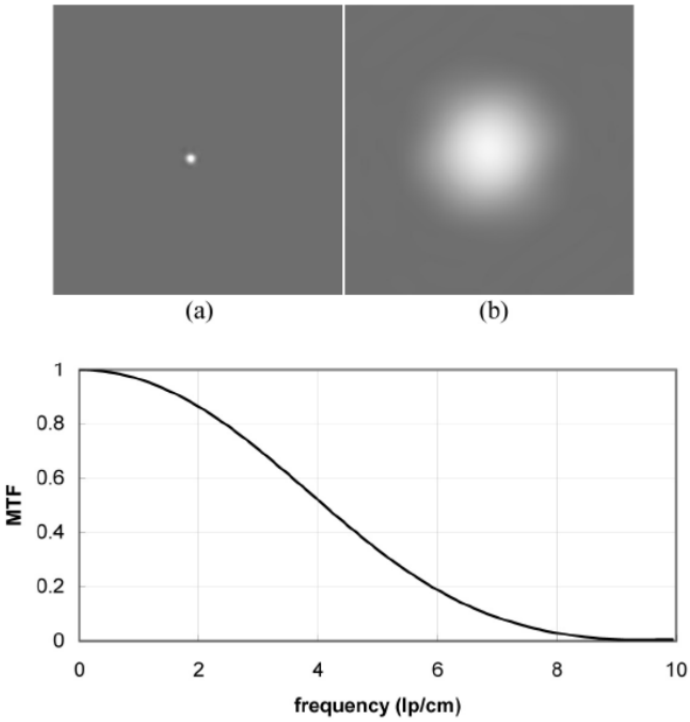

Figure 15. Example of a wire scan and MTF measurement. (a) Tungsten wire reconstructed with the standard algorithm to approximate PSF. (b) Magnitude of the Fourier transform of the PSF image. In this example, the MTF curve is the averaged magnitude over 360 degrees [5]

For most XCT instruments a single MTF curve is acquired by averaging the MTF function over a 360 degree range. The spatial resolution is mostly specified in terms of the frequency for a given per cent value of the MTF, such as 50 %, 10 % or 0 % MTF [5], [14].

Methods for obtaining the MTF from the PSF are also described elsewhere [31], [33], [34], [35], [36]. A number of problems and disadvantages of these methods were reported. For example, since the wire is very thin, only a few pixels lie in its vicinity, making the PSF highly undersampled. It is, therefore, required to perform the reconstruction of the wire measurement with a very small number of pixels. However, the measured PSF does not completely correspond to a typical XCT image that is reconstructed using larger pixels. Some iterative algorithms do not even allow reduction of the pixel size to arbitrary small values without significantly changing their spatial resolution characteristics and considerably increasing the reconstruction time [37].

Another example of a drawback includes a standard filtered backprojection [38], used in most XCT instruments. Here an anti-aliasing Moiré filter is applied to suppress frequencies that cannot be represented by the pixels; this filter has a cut-off frequency depending on the pixel size. For such cases the wire method is not applicable, since changing the pixel size also changes the shape of the PSF [37]. The study of the impact of a wire diameter on the measurement of the PSF was also discussed elsewhere [35]. Another issue is that the value and shape of the PSF depend not only on the size of the test object but also on the material it is made from [39].

It is assumed that in XCT instruments the PSF possesses rotational symmetry and is space invariant. This assumption has been investigated [40]. It was found that the PSF had a tendency to broaden with increased distance from the centre of the field of view (FOV), leading to a slight loss of resolution. Also, as the distance from the centre increased, the shape of the cross-section of the PSF became elliptical instead of circular, losing its radial symmetry. Taking into account the properties of the Fourier transform [41], the Fourier transform of such an asymmetric PSF is no longer the MTF alone but the OTF with a non-zero PTF component.

Just as in the case of the line-pair test patterns, the phantoms that contain thin wires to simulate the response of the imaging system to a point source have a high manufacturing cost. Additional difficulties with the method of obtaining the MTF from the PSF are discussed elsewhere [42].

In order to avoid some of the difficulties associated with the calculation of the PSF, the MTF can be obtained from the line spread function (LSF). The LSF represents the radiation intensity distribution of an infinitely narrow and infinitely long slit of unit density [4]. It can be shown that the one-dimensional profile of a circularly symmetric PSF is roughly equivalent to a profile taken perpendicular to the two-dimensional response of the imaging system to a line [13]. For a narrow line object parallel to the y-axis, the LSF is related to the PSF by the equation [1]

$$\mathrm{LSF}\,(x) = \int_{-\infty}^{\infty} \mathrm{PSF}(x, y)\mathrm{dy}. \tag{19}$$

In practice, the LSF is measured by approximating a line source with a slit which is narrow and long relative to the size of the PSF [43], [44], [45]. Two clear advantages of calculating the LSF are that it is practically easier to approximate a line than a point; and in imaging a line, more pixels are used, which results in a better signal-to-noise ratio. However, since the LSF depends on the orientation of the line object [3], the method for calculating the MTF from the LSF can be applied only if the PSF is assumed to be rotationally symmetric.

4.3 CALCULATING THE MTF USING THE EDGE RESPONSE FUNCTION

Another method for calculating the MTF is from the LSF using the edge response function (ERF). The ERF is the response of an imaging system to a vertical attenuating edge. Mathematically, the ERF, for an edge parallel to the y-axis is related to the LSF by the equation [1]

$$\mathrm{ERF}\,(x) = \int_{-\infty}^{x} \mathrm{LSF}(x')\mathrm{dx}'. \tag{20}$$

The experimental procedure for obtaining the MTF from the ERF is outlined elsewhere [13], [15], [46]. A simple cylinder is imaged (figure 16a), many profiles through its centre of mass are aligned and averaged to reduce system and quantization noise, and the ERF is calculated (figure 16b). The LSF is then estimated by taking the discrete derivative of the ERF (figure 16c); its discrete Fourier transform is taken to obtain the MTF (figure 16d).

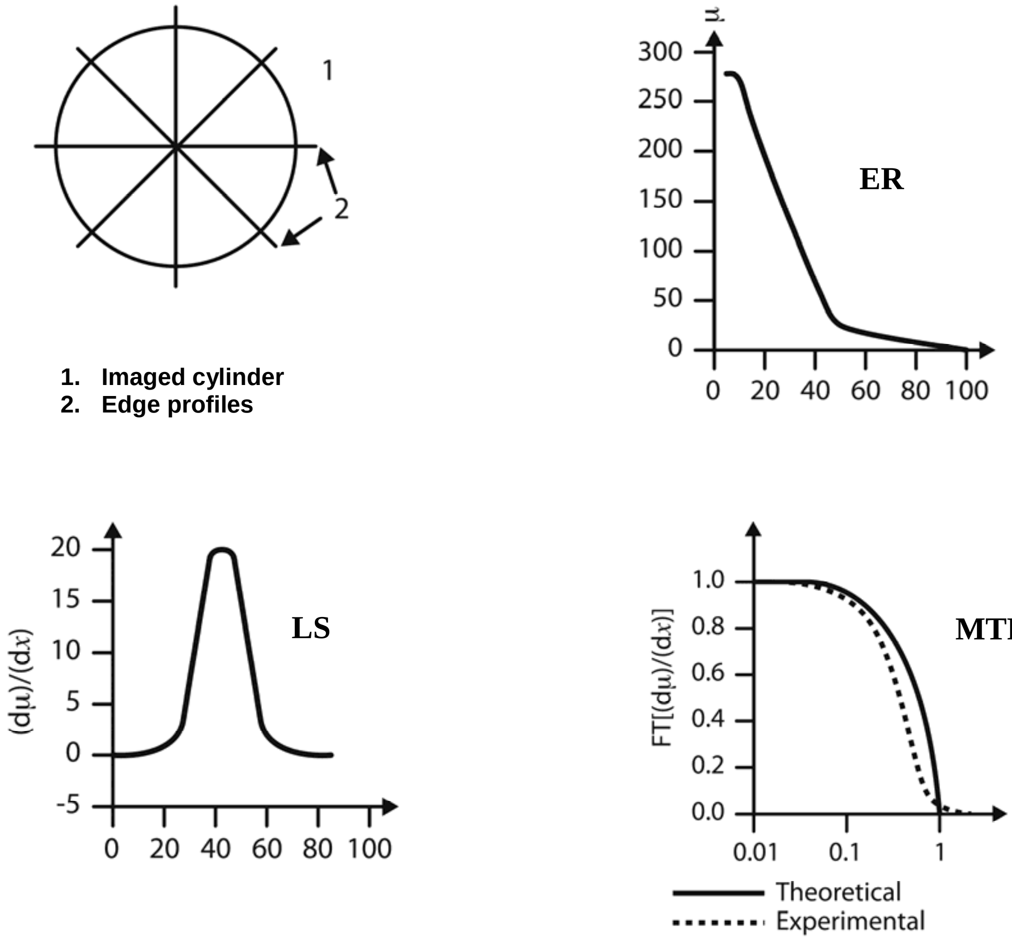

Figure 16. Illustration of the procedure for obtaining the MTF from a CT image of a small cylinder. a) sketch indicating relative orientation of three different line profiles through the centre of the imaged cylinder; b) result of aligning and averaging many edge profiles, the ERF; c) system LSF; d) system calculated MTF [13]

Figure 17 presents the summary of this process.

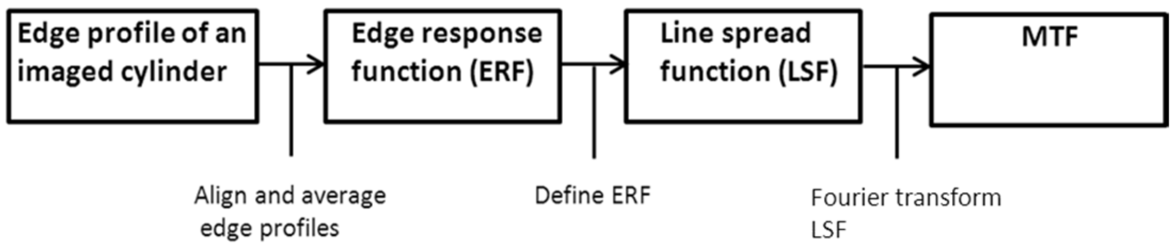

Figure 17. Example test procedure for obtaining the MTF [12]

A variation of this method is described elsewhere [46]. A composite profile of the edge of the disk is generated from the CT image data to obtain the ERF. The derivative of the ERF is calculated to obtain the PSF. The amplitude of the Fourier transform of the PSF is calculated to obtain the MTF.

The method of calculating the MTF from the ERF has several advantages. For example, practically it is much easier to generate an edge in the image, rather than an ideal line or point object [47], [48]. All common edge responses have a similar shape, even though they may originate from very different PSFs. The MTF can be directly found by taking the one-dimensional Fourier transform of the LSF (unlike the PSF to the MTF calculation that must use a two-dimensional Fourier transform) [49].

4.4 CALCULATING THE MTF FROM THE LINE-PAIR TEST PATTERNS

The line-pair test patterns that are used for direct estimation of the spatial resolution of imaging systems (described in section 3.2.1) can also be used for calculating the MTF of these systems. Figures 18 and 19 demonstrate two examples of such test patterns.

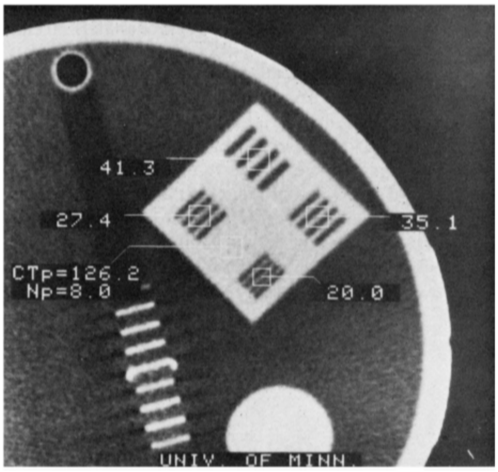

Figure 18. Test bar pattern [50]

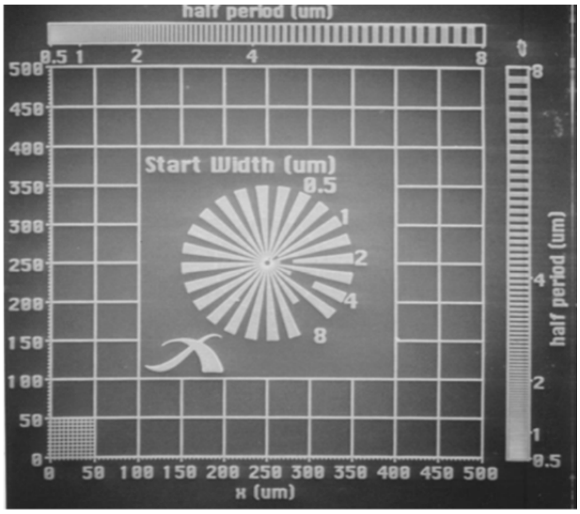

Figure 19. Test pattern Xradia X500-200-30 [51]

The method of calculating the MTF from the line-pair test patterns relies on the measurement of the modulation *M*. The average intensity profile along the test bar pattern is analysed to determine the peaks and troughs (I_{max} and I_{min}) and their location (n_{max} and n_{min}). The modulation of the peak-trough pair is calculated using equation (12).

The spatial frequency for each pair in lines per millimetre is given by

$$f = \frac{1}{d} \times 1000\,. \tag{21}$$

Calculated values of the modulation at different spatial frequencies are then used to produce the MTF [52].

A variation of the above method is described elsewhere [29], where the contrast factor *R* is calculated as a function of spatial frequency. The line-pair test structures (figure 20) were imaged with an instrument.

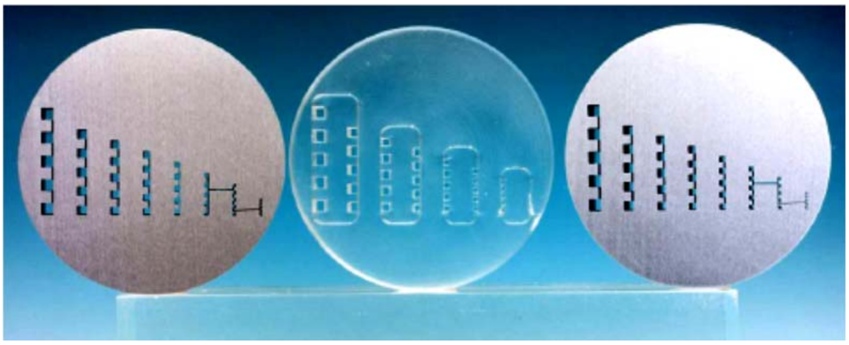

Figure 20. Test structures made from three different materials, with eight different sized structures ranging from 0.4 mm to 2.5 mm, corresponding to the spatial resolution of 1.25 line-pairs per millimetre to 0.2 line-pairs per millimetre [29]

The contrast is then measured at a grey-value profile along a line in the reconstructed volume, where the grey-value minima $N_A\,(i)$ are determined in the cut-outs and the maxima $N_B\,(i)$ in the material bridges (figure 21).

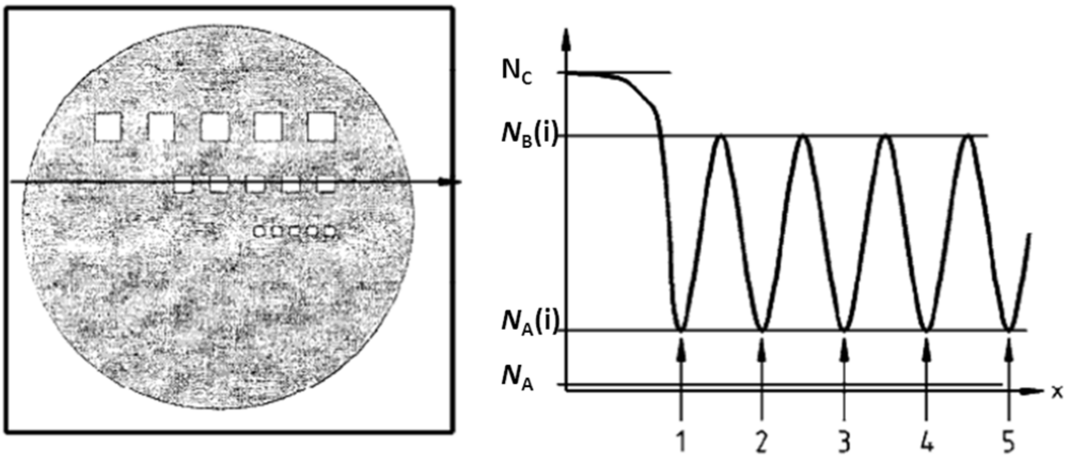

Figure 21. Determination of grey-value extrema at the line-pair structures [29]

The contrast factor $R(i)$ is the difference between $N_B\,(i)$ and $N_A\,(i)$, normalised to the grey-value difference of the material N_A and the background N_C

$$R(i) = \frac{N_B\,(i) - N_A\,(i)}{N_C - N_A} \times 100\,. \tag{22}$$

The MTF can also be calculated from the line-pair test patterns using Coltman's equation, and is often referred to as the square wave response function method (SWRM) [45]. Coltman's equation calculates the sine wave response factor $R(n)$, defined as the ratio of the amplitude of the output sine wave to that of the input wave, from the square wave response factor, $r(n)$, where n is the spatial frequency [53]. Examples of this approach are found elsewhere [45], [50], [54]. This method is based on the fact that the sine wave response, which is readily manipulated but difficult to measure, may be obtained from the square wave response, which can be easily obtained experimentally. In SWRM the $R(n)$ has to be calculated for a number of spatial frequencies from which the MTF is then estimated.

Although the method for calculating the MTF from the line-pair test patterns can be considered simpler than the methods for calculating the MTF from the PSF or from the ERF, requiring no special software [50], there are several limitations. One of the main limitations is that the modulation value or the sine wave response factor has to be calculated separately for each spatial frequency. As a result, in order to produce the MTF, a large number of calculations have to be performed. Another difficulty is that the test structures of high spatial frequency, with sizes much lower than one millimetre are difficult, if not impossible, to manufacture [29].

5. OBTAINING THE MTF IN THE *Z*-AXIS

The previous three methods for calculating the MTF are applied to the *x/y*-scan plane. To describe the spatial resolution in the *z*-axis the slice sensitivity profile (SSP) is used. Similar to in-plane resolution, the SSP describes the system response to a Dirac delta function $\delta(z)$ in the *z*-axis.

In practice, the Dirac delta function is often approximated by objects with a thickness that is significantly smaller than the slice thickness of the data acquisition. For example, researchers use a small bead or a thin disc, known as delta phantoms, to perform SSP measurements [14]. These phantoms are mainly used in spiral XCT. For conventional XCT, a more convenient method of measuring SSP is to use a shallow-angled slice ramp phantom. These are usually implemented in the form of thin strips, such as aluminium with a thickness of 0.1 mm, attached at a particular angle with respect to the *z*-axis. The use of ramp phantoms allows the slice profile to be measured quickly; the profile is determined directly in the image and then evaluated. However, ramp phantoms do not produce reliable results for spiral XCT [55].

The specification for the spatial resolution in z is given by the full width at half maximum (FWHM) or full width at one tenth of maximum (FWTM), both of which are illustrated in figure 22 [5].

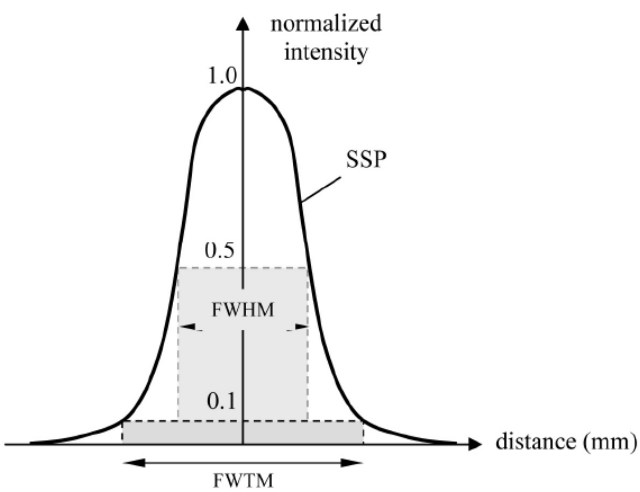

Figure 22. Illustration of FWHM and FWTM. FWHM represents the distance between two points on the SSP curve whose intensity is 50 % of the peak. FWTM represents the distance between two points on the SSP whose intensity is 10 % of the peak [5]

The shape of the SSP has a considerable influence on the imaging of smaller object details. The contrast of an object, which is smaller than the slice thickness, and located only partly in the scanned slice, is reduced according to the extent to which it is positioned in the particular volume element (see figure 23) [14].

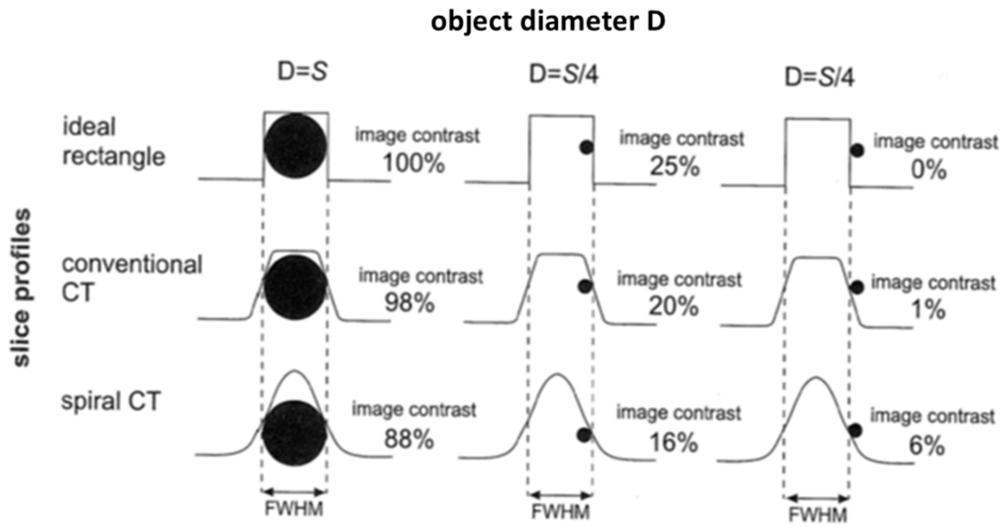

Figure 23. Influence of the SSP shape on imaging small objects (adapted from [14])

Since the shape of the profile is not represented in the FWHM value, other variables have been proposed. These include, full width at tenth area (FWTA), which is the width of the profile at a height which includes 90 % of the area under the profile and excludes 10 % [56], and the slice profile quality index (SPQI) [57], where

$$\mathrm{SPQI} = \frac{\text{Area bounded by the nominal slice width}}{\text{Area of ideal profile}} \cdot 100\ \% \, . \tag{23}$$

The use of FWHM and FWTM instead of calculating the MTF is due to historical, not technical reasons. In the past, XCT images were generally reconstructed with thicker slices in the range of 5 mm to 10 mm, and FWHM and FWTM were easy to measure and describe for these images. With recent technological advancements there is no valid reason why the MTF cannot be used to fully characterize the system performance in the z-axis [5].

Although it is still common practice to measure lateral and longitudinal spatial resolution separately, a method where 3D resolution is determined with just one scan is described elsewhere [37]. A sphere much larger than the spatial resolution of the system was used. The benefits of using a large sphere were described as follows: the large diameter of the sphere allows it to be locally approximated by a planar edge, such spheres can be manufactured to a very high accuracy in radius and form, the location of the sphere can be easily extracted from a reconstructed volume and only a single measurement is required to access the lateral and the longitudinal PSFs without specific requirements on the voxel size selected during reconstruction. It was concluded that this method appears to be superior to other existing methods.

6. DISCUSSION AND CONCLUSIONS

The purpose of this review was to summarise and discuss the current application of the optical transfer function concept in XCT. A brief introduction to the relationship between the OTF, the MTF and the PTF was given. For the OTF to be valid, the imaging system must be linear and space invariant. For XCT this would imply, for example, that a change in the input variable, the linear attenuation coefficient μ, has to be reflected in an equivalent change in the output variable. However, due to such factors as the polychromatic nature of the X-ray beam and the energy dependency of μ, which causes well-known beam hardening [13], Compton scattering [5], quantum noise, detector characteristics [14], *etc.*, the linearity of the imaging system is compromised. Although, there are a number of publications discussing the importance of correcting for beam hardening and other non-linear influences in, for example [11], [47], [58], [59], further work is needed to investigate how such factors affect the OTF.

In most cases only the MTF part of the OTF is used to describe the performance of an imaging system. One of the reasons is the assumption that in XCT the PSF possesses rotational symmetry, and hence, the PTF part is zero. Some studies have proved such assumptions to be incorrect [39], [40]. Another suggested reason for omitting the PTF is that significant changes in the PTF predominantly occur at higher spatial frequencies where the MTF had fallen to relatively low levels and that the effect of the phase changes has limited impact on the image quality [1]. This does not appear to be a valid enough reason not to investigate the impact of the PTF on spatial resolution.

The OTF is the transfer function of a spatially incoherent imaging system. In industrial XCT imaging systems, the X-ray source is polychromatic in nature and is, therefore, assumed to be spatially and temporally incoherent. However, in practice it is more likely to be partially coherent, due to, for example, the finite size of the focal spot, or the presence of a pinhole, and the spectral bandwidth. Further investigations into the degree of coherence of the X-ray source are needed.

There are three main ways for calculating the MTF of an XCT system: from the PSF, from the ESF and through imaging the line-pair test patterns. Each method has its own advantages and disadvantages. Several researchers have compared the two methods [29], [45]. However, no direct comparison of all three methods has been identified in this review. It is, therefore, proposed to carry out such a study, in order to investigate the impact of different methods on the MTF values.

Numerous factors affect the overall performance of XCT systems and the spatial resolution in particular: focal spot size, pixel and voxel size, geometrical variables of the system, reconstruction algorithms, *etc.* A number of papers attempt to classify these parameters and discuss improvement strategies to increase the accuracy of measurements [5], [14], [60], [61], [62]. A recently conducted comparison study (“CT Audit”) involving fifteen XCT systems from several laboratories in Europe, America and Asia, reported a variety of problems that occur when using XCT systems for the purposes of dimensional metrology [63]. For example, XCT measurement results obtained from the calibrated items demonstrate that for XCT systems form measurements are more problematic than measurements of size quantities, such as distance and diameter measurements. A general comment on the CT Audit results, was that the participants had difficulties in evaluating the measurement uncertainty appropriately, showing that the traceability of dimensional XCT measurements is still a major challenge.

Although several attempts have been made to standardise practices for assessing the performance of XCT systems [13], [15], [64], there is currently no internationally accepted specification standard which provides a comprehensive guide for calibration and verification of XCT systems [12]. It was noted that in the literature the two terms are frequently used interchangeably, but it is important to distinguish between them. Calibration is the process of comparing the measurement result obtained from the instrument under investigation against that of a known standard, which has an unbroken chain back to national or international standards, with each comparison having a stated uncertainty. Verification is analogous to calibration but returns only a pass/fail result that indicates whether the instrument is operating within a defined specification [12]. At present, XCT system verification relies mostly on the use of specially designed test or reference objects [60], [65], [66]; whilst calibration predominantly focuses on the individual influence factors of the system, such as the characteristics of the focal spot or system geometry [67], [68], [69].

At NPL research is underway to develop techniques for establishing calibration standards in 3D imaging and surface topography measurements using the OTF approach [30], [70]. It would be interesting to investigate whether a similar OTF approach could be used for calibration of the XCT imaging systems.

REFERENCES

[1] Williams T 1999 *The optical transfer function of imaging systems* (IOP Publishing Ltd)

[2] Williams C S and Becklund O A 2002 *Introduction to the optical transfer function* (SPIE Press)

[3] Metz C E and Doi K 1979 Transfer function analysis of radiographic imaging systems *Phys. Med. Bio.* **24** 1079–1106

[4] Rossmann K 1969 Point spread function, line spread function and modulation transfer function *Radiology* **93** 257–272

[5] Hsieh J 2009 *Computed tomography: principles, design, artifacts and recent advances* (SPIE Press)

[6] Pfeiffer F, Weitkamp T, Bunk O and David C 2006 Phase retrieval and differential phase-contrast imaging with low-brilliance X-ray sources *Nature Physics* **2** 258–261

[7] Wolf E 2007 *Introduction to the theory of coherence and polarization of light* (Cambridge University Press)

[8] den Dekker A J and van den Bos A 1997 Resolution: a survey *J. Opt. Soc. Am.* **14** 547–556

[9] Goodman J W 2005 *Introduction to Fourier optics* (Roberts & Company Publishers)

[10] Carmignato S 2012 Accuracy of industrial computed tomography measurements: experimental results from an international comparison *Ann. CIRP* **61/1** 1–4

[11] Kruth J P, Bartscher M, Carmignato S, Schmitt R, De Chiffre L and Weckenmann A 2011 Computed tomography for dimensional metrology *Ann.CIRP* **60** 821–842

[12] Sun W, Brown S B and Leach R K 2012 An overview of industrial X-ray computed tomography *NPL Report* **ENG32**

[13] ISO 15708-1 2002 Non-destructive testing - radiation methods - computed tomography. Part 1: principles (International Organization for Standardization)

[14] Kalender W 2011 *Computed tomography: fundamentals, system technology, image quality, applications* (Publicis Publishing)

[15] E 1441-00 2000 Standard guide for computed tomography (CT) Imaging (ASTM International)

[16] Ketcham R A and Carlson W D 2001 Acquisition, optimization and interpretation of X-ray computed tomographic imagery: applications to the geosciences *Computers & Geosciences* **27** 381–400

[17] Seibert J A and Boone J M 2005 X-ray imaging physics for nuclear medicine technologists. Part 2: X-ray interactions and image formation *J. Nucl. Med. Technol.* **33** 3–18

[18] Schuster A 2012 *An introduction to the theory of optics* (Forgotten Books)

[19] Houston W V 1927 A compound interferometer for fine structure work *Phys. Rev.* **29** 478–484

[20] Buxton A 1937 Note on optical resolution *Philos. Mag.* **23** 440–442

[21] Born M and Wolf E 1980 *Principles of Optics: Electromagnetic theory of propagation interference and diffraction of light* (Cambridge University Press)

[22] Hecht E 1987 *Optics* (Addison-Wesley Publishing Company)

[23] Lord Rayleigh 1902 *Collected papers* (Cambridge University Press) **3** 85

[24] Barakat R 1962 Application of apodization to increase two-point resolution by the Sparrow criterion. I. Coherent illumination *J. Opt. Soc. Am.* **A52** 276–283

[25] Lummer O and Reiche F 1910 *Die lehre von der bildentstehung im mikroskop* (von Ernst Abbe, Braunschweig)

[26] Luneberg R K 1944 *Mathematical theory of optics* (Brown University)

[27] Ronchi V 1961 Resolving power of calculated and detected images *J. Opt. Soc. Am.* **A51** 458–460

[28] Japan Inspection Instruments Manufacturers' Association (JIMA) 2012 Micro resolution chart for X-ray Website: www.jima.jp/content/pdf/rt_ct-02cata02.pdf Accessed on 23 July 2012

[29] Staude A and Goebbels J Determining the spatial resolution in computed tomography – comparison of MTF and line-pair structures Website: www.dir2011.com/Portals/dir2011/BB/tu41.pdf Accessed on 12 June 2012

[30] Foreman M R, Giusca C L, Leach R K and Coupland J M 2012 Determination of the transfer function for optical surface topography measuring instruments *NPL Report* **MS1**

[31] Ohkubo M, Wada S, Ida S, Kunii M, Kayugawa A, Matsumoto T, Nishizawa K and Murao K 2009 Determination of point spread function in computed tomography accompanied with verification *Med. Phys.* **36** 2089–2097

[32] Solomon C and Breckon T 2010 *Fundamentals of digital image processing: a practical approach with examples in Matlab* (Wiley-Blackwell)

[33] Glover G H and Eisner R L 1979 Theoretical resolution of computed tomography systems *J. Comput. Assist. Tomogr.* **3** 85–91

[34] Bischof C J and Ehrhardt J C 1977 Modulation transfer function of the EMI CT head scanner *Med. Phys.* **4** 163–167

[35] Nickoloff E L 1988 Measurement of the PSF for a CT scanner: appropriate wire diameter and pixel size *Phys. Med. Bio.* **33** 149–155

[36] Joseph P M, Spital R D and Stockham C D 1980 The effects of sampling on CT images *Comput. Tomogr.* **4** 189–206

[37] Grimmer R, Krause J, Karolczak M, Lapp R and Kachelrieß M 2008 Assessment of spatial resolution in CT *Nuclear Science Symposium Conference IEEE conference publications* 5562–5566

[38] Kak A C and Slaney M 2001 *Principles of computerized tomographic imaging* (SIAM)

[39] Chen Z and Tao Y 2008 Effects of digital geometry and phantom size on cone-beam CT point spread function measurement *Proc. SPIE* **6913** 50–1 - 50–11

[40] Dore S and Goussard Y 1997 Experimental determination of CT point spread function anisotropy and shift-variance *19th International Conference IEEE/EMBS* 788–791

[41] Woan G 2000 *The Cambridge handbook of physics formulas* (Cambridge University Press)

[42] Cheng Z and Ning R 2005 Pitfalls in point-spread-function measurement of computed tomographic system by microphantom reconstruction *Opt. Eng.* **44** 017002–1 - 017002–8

[43] Fujita H, Tsai D Y, Itoh T, Doi K, Morishita J, Ueda K and Ohtsuka A 1992 A simple method for determining the modulation transfer function in digital radiography *IEEE Transact. Med. Imag.* **11** 34–39

[44] Boone J M 2001 Determination of the presampled MTF in computed tomography *Med. Phys.* **28** 356–360

[45] Morishita J, Doi R, Bunch P, Hoeschen D, Sirand-rey G and Sukenobu Y 1995 Comparison of two methods for accurate measurement of modulation transfer functions of screen-film systems *Med. Phys.* **22** 193–200

[46] E 1695-95 2006 Standard test method for measurement of computed tomography (CT) system performance (ASTM International)

[47] Casteele E V D, Dyck D V, Sijbers J and Raman E 2004 The effect of beam hardening on resolution in X-ray microtomography *Proc. SPIE* **5370**

[48] Bentzen S M 1983 Evaluation of the spatial resolution of a CT scanner by direct analysis of the edge response function *Med. Phys.* **10** 579–581

[49] Smith S W 1997 *The scientist & engineer's guide to digital signal processing* (California Technical Publishing)

[50] Droege R T and L M R 1982 A practical method to measure the MTF of CT scanners *Med. Phys.* **9** 758–760

[51] Xradia resolution test patterns Website: www.xradia.com/products/xray-optics/resolution-targets.php Accessed on 15 August 2012

[52] Sharma K S, Seshadri S, Feser M and Wang G 2010 Accurate resolution measurement for X-ray micro-CT systems *10th International Conference on X-ray Microscopy* (*AIP Conference Proceedings*) 337–340

[53] Coltman J 1954 The specification of imaging properties by response to a sine wave input *J. Opt. Soc. Am.* **44** 468–471

[54] Hassan W M S W 2002 Calculation of the modulation transfer function from the square wave response function data with an interactive curve fitting software *Physica Medica* **18** 25–31

[55] Polacin A, Kalender W, Brink J and Vannier M 1999 Measurement of slice sensitivity profiles in spiral CT *Med. Phys.* **21** 133–140

[56] Polacin A, Kalender W A and Marchal G 1992 Evaluation of section sensitivity profiles and image noise in spiral CT *Radiology* **185** 29–35

[57] Kalender W 1995 *Principles and performance of spiral CT. In Medical CT and ultrasound: current technology and applications* (Madison, Wisconsin: Advanced Medical Publishing)

[58] van de Casteele E 2004 *Model-based approach for beam hardening correction and resolution measurements in microtomography* (Universiteit Antwerpen)

[59] Duerinckx A J and Macovski A 1979 Nonlinear polychromatic and noise artifacts in X-ray computed tomography images *J. Comput. Assist. Tomogr.* **3** 519–526

[60] Kiekens K, Welkenhuyzen F, Tan Y, Bleys P, Voet A, Dewulf W and Kruth J-pierre 2010 A test object for calibration and accuracy assessment in X-ray CT metrology *10th International Symposium on Measurement and Quality Control Meas. Sci Technol.* **22** 1–4

[61] Muller P 2011 Influence parameters in CT scanning Website: orbit.dtu.dk/fedora/objects/orbit:113388/datastreams/file_9889775/content Accessed on 23 July 2012

[62] Welkenhuyzen F, Kiekens K, Pierlet M, Dewulf W, Bleys P and Voet A 2009 Industrial computer tomography for dimensional metrology: overview of influence factors and improvement strategies *International Conference on Optical Measurement Techniques for Structures and Systems* Optimess edition: 4 1–9

[63] Carmignato S, Pierobon A and Savio E 2011 CT Audit: Interlaboratory comparison of computed tomography systems for dimensional metrology Website: static.gest.unipd.it/~carmignato/ct-audit/index.htm Accessed on 24 August 2012

[64] VDI/VDE 2630 2010 Computed tomography in dimensional metrology. Measurement procedure and comparability (Beuth)

[65] Kiekens K, Welkenhuyzen F, Tan Y, Bleys P, Voet A, Kruth J-P and Dewulf W 2011 A test object with parallel grooves for calibration and accuracy assessment of industrial computed tomography (CT) metrology *Meas. Sci. Technol.* **22** 115502

[66] Carmignato S, Dreossi D, Mancini L, Marinello F, Tromba G and Savio E 2009 Testing of X-ray microtomography systems using a traceable geometrical standard *Meas. Sci. Technol.* **20** 1–4

[67] Panetta D, Belcari N, Del Guerra A and Moehrs S 2008 An optimization-based method for geometrical calibration in cone-beam CT without dedicated phantoms *Phys. Med. Bio.* **53** 3841–3861

[68] Yang K, Kwan A L C and Miller D F 2010 A geometric calibration method for cone beam CT systems *Med. Phys.* **33** 1695–1706

[69] Cho Y, Moseley D J, Siewerdsen J H and Jaffray D A 2005 Accurate technique for complete geometric calibration of cone-beam computed tomography systems *Med. Phys.* **32** 968–983

[70] Leach R K, Giusca C L and Coupland J M 2012 Advances in calibration methods for micro- and nanoscale surfaces *Proc.* SPIE **8430** 1–9